Available online at www.sciencedirect.com
SCIENCE DIRECT
Remote Sensing of Environment 97 (2005) 447 – 457
Remote Sensing of Environment
www.elsevier.com/locate/rse

Global mapping of foliage clumping index using multi-angular satellite data

J. M. Chen [a,*], C. H. Menges [a], S. G. Leblanc [b]

[a] Department of Geography and Program in Planning, University of Toronto, 100 St. George Street, Room 5047, Toronto, Ontario, Canada M5S 3G3
[b] Earth Observation Applications and Advisory Section, Canada Centre for Remote Sensing, 588 Booth Street, Ottawa, Ontario, Canada K1A 0Y7

Received 8 November 2004; received in revised form 19 April 2005; accepted 8 May 2005

Abstract

Global mapping of the vegetation clumping index is attempted for the first time using multi-angular POLDER 1 data based on a methodology that has been demonstrated to be applicable to Canada's landmass. The clumping index quantified the level of foliage grouping within distinct canopy structures, such as tree crowns, shrubs, and row crops, relative to a random distribution. Vegetation foliage clumping significantly alters its radiation environment and therefore affects vegetation growth as well as water and carbon cycles. The clumping index is useful in ecological and meteorological models because it provides new structural information in addition to the effective LAI retrieved from mono-angle remote sensing and allows accurate separation of sunlit and shaded leaves in the canopy. The relationship between an angular index (normalized difference between hotspot and darkspot) and the clumping index is explored using a geometrical optical model named "4-Scale". A simplified version of the mechanistic hotspot model used in 4-Scale is developed to derive the hotspot reflectance from multi-angle measurements for mapping purposes. An accurate clumping map for areas with significant tree (shrub) covers has been achieved, although further research is required to reduce topographic effects.

Keywords: Multi-angle remote sensing; Vegetation clumping index; POLDER; LAI; Hotspot; Angular index; BRDF

1. Introduction

Vegetation covers on the earth surface have different structures, and the foliage has different degrees of organization depending on the cover type. Conifer forests may be most highly organized with structures such as shoots, branches, whorls, tree crowns and tree groups, while grasses and crops are lacking similar structures. In canopies with these structures, the distribution of foliage is spatially confined and therefore not random. The confined distribution of foliage in these structures is referred to as clumping (Chen & Black, 1992). Through Markov chain analysis, Nilson (1971) first defined a vegetation dispersion parameter Ω as a modification to Beer's law:

$$P(\theta) = e^{-G(\theta)L\Omega/\cos\theta} \quad (1)$$

where $P(\theta)$ is the probability of the transmission of a beam of light at the zenith angle θ through the canopy, i.e., the gap fraction; $G(\theta)$ is the extinction coefficient, being 0.5 for canopies with a random distribution of leaf angles; and L is the leaf area index, which is most commonly defined as one half the total (all sided) leaf area per unit ground surface area when leaves are of convex shapes (Chen & Black, 1992). The dispersion parameter Ω is determined by the spatial distribution pattern of leaves. If the distribution is random, it is unity, and Eq. (1) returns to the original Beer's law. If the distribution is not random, it can be larger or smaller than unity. In the case that the leaf distribution is more regular (leaves side by side) than random, the Ω value is larger than unity, so the same L intercepts more radiation, making $P(\theta)$ smaller. In the case that the leaf distribution is more clumped (leaves on top of each other) than random, the Ω value is smaller than unity, so the same L intercepts less radiation, making $P(\theta)$ larger. As most natural canopies are clumped, Ω is often directly called "clumping index"

* Corresponding author. Tel.: +1 416 978 7085.
E-mail address: chenj@geog.utoronto.ca (J.M. Chen).

0034-4257/$ - see front matter © 2005 Elsevier Inc. All rights reserved.
doi:10.1016/j.rse.2005.05.003

(Chen & Black, 1992). The more clumped a canopy is, the smaller is the Ω value.

In remote sensing applications, foliage clumping has at least two significances. First, it affects the gap fraction $P(\theta)$ for the same LAI, which is often derived as a function of a vegetation index, such as the NDVI or the simple ratio (Chen et al., 2002; Running et al., 1994; Sellers et al., 1994). These indices are generally proportional to foliage cover (or 1-gap fraction) in the view direction, and therefore are influenced by clumping. Clumping can also delay the occurrence of the saturation in reflectance as LAI increases (Bacour et al., 2001; Chen et al., 2002; Gobron et al., 1997). Second, it affects both radiation interception and distribution within the canopy, which in term affect photosynthesis (Baldocchi et al., 2002; Bernier et al., 2001; Chen et al., 1999; Liu et al., 2002; Palmroth & Hari, 2001; Stenberg, 1998; Walcroft et al., in press) and evapotranspiration (Liu et al., 2003). Chen et al. (2003) reported that the maximum net and gross primary productivities of a boreal black spruce forest as modeled by the Boreal Ecosystem Productivity Simulator (BEPS) were reached for a clumping index of 0.5 because of large contributions from shaded leaves, suggesting that the clumping of foliage is ecologically significant. This structural effect on productivities may be interpreted as a mechanism to optimize the within-crown radiative regime for growth (Cescatti, 1998). The estimation of daily canopy photosynthesis can differ by 20% for black spruce when clumping is considered (Lacaze et al., 2002).

The essential information contained in optical remote sensing measurements made at a single angle is the canopy gap fraction or its inversion: the effective LAI, taken as the product of LAI and the clumping index (Chen, 1996). While it is possible to assign a single clumping value to each cover type in LAI algorithms as in the operational derivation of LAI from MODIS (Wang et al., 2004), this does not account for its spatial variation and relies on biome classification and the level of abstraction inherent in the classification procedure. Mapping of the clumping index is therefore desirable to improve the representation of vegetation structure in modeling carbon and water cycles of terrestrial ecosystems.

Multi-angular satellite observations provide a means to characterize the anisotropy of surface reflectance, which has been shown to contain information on the structure of vegetated surfaces (Chen et al., 2003; Cierniewski et al., 2004; Deering et al., 1999; Gao et al., 2003; Rautiainen et al., 2004; Sandmeier & Deering, 1999; Zhang, Tian, Myneni et al., 2002, Zhang, Shabanov et al., 2002). The total reflectance measured by a single observation at nadir is largely determined by the sunlit components. Utilizing similar measurements over a range of observation angles, however, allows estimation of the proportion of shaded foliage components from the pattern of variation. For mapping purposes using multiple angle data, the challenge arises in characterizing the bidirectional reflectance distribution function (BRDF) with a single value. Sandmeier and Deering (1999) proposed the anisotropy factor (ANIF), which is simply a normalization of the directional reflectance with respect to the nadir reflectance at a given wavelength, and the anisotropy index (ANIX), which is the simple ratio of the maximum and minimum bidirectional reflectance at given measurement angles. Both were found to capture the structural information of boreal forest species, although ANIF requires a comparable solar angle, and ANIX suffered from the problem of identifying the reflectance at the hotspot from remotely sensed observations directly. This is problematic because the observed reflectance is highly sensitive to small angle changes near the hotspot.

The Normalized Difference between Hotspot and Darkspot (NDHD) has been proposed as an angular index to characterize the anisotropic behavior, and it has been successfully related to ground based measurements of the clumping index (Chen et al., 2003). It is defined as:

$$\mathrm{NDHD} = \frac{\rho_h - \rho_d}{\rho_h + \rho_d} \tag{2}$$

where ρ_h and ρ_d are the reflectance at the hotspot and darkspot, respectively. This is essentially the same index as ANIX but the hotspot reflectance is derived from the available observations through model interpolation. It is slightly different from the hotspot and darkspot index, $\mathrm{HDS}=(\rho_h-\rho_d)/\rho_d$, proposed earlier by Chen et al. (2001) and Lacaze et al. (2002). Chen et al. (2003) found that NDHD is more linearly related to clumping index than HDS. Leblanc, Chen, White et al. (in press) use NDHD for mapping clumping of Canada's landmass.

The hotspot is a geometric-optical effect denoting the backscatter peak in directional reflectance when illumination and view directions coincide, resulting in the absence of visible shadows (Hapke et al., 1996). Most of the clumping information, however, is contained in the darkspot reflectance, which contains a maximum of visible shadows observed in the forward scattering direction, where the reflectance is minimum (Gerard & North 1997; Chen & Leblanc, 1997). At this point the recorded reflectance is determined by the density of the foliage as well as the vertical and horizontal extents of foliage structures and thus the level of clumping. Using the relative magnitude of the darkspot to the hotspot minimizes the dependence of the index on foliage optical properties that are important determinants of bidirectional reflectance (Asner et al., 1998; Panferov et al., 2001).

The first part of this paper presents the analysis of the relationship between NDHD and the vegetation clumping index using a geometrical optical model to simulate the effects of a large range of parameters that can be expected in global vegetation covers. The second part of this paper describes the global application of the algorithm to remotely sensed satellite data. The POLDER sensor onboard the Japanese platform ADEOS records reflectance values in four frequency ranges over a large range of view angles within a

single overpass to allow derivation of BRDFs. The POLDER-1 instrument was launched onboard the ADEOS platform in August 1996. The instrument acquired data almost continuously from October 1996 to June 1997 when the platform solar panel failure terminated its operation. POLDER observations were chosen for the derivation of the angular index NDHD because it provides measurements near the principal plane where BRDF effects are most pronounced (Sandmeier & Deering, 1999). While MISR is an operational sensor providing high quality calibrated multi-angular measurements (Diner et al., 2002), its design and orbit limits observations along the principal plane. Although sub-pixel vegetation structure has been successfully derived from MISR measurements through the extrapolation of background vs. foliage contributions over the angular range (Gobron et al., 2002; Pinty et al., 2002), the effect was found to be detectable only for high resolution data that makes it difficult for global mapping purposes.

2. Methodology

The relationship between the clumping index and the angular index NDND is investigated using the 4-Scale model (Chen & Leblanc, 1997; Leblanc et al., 1999). Using geometric-optical and radiative transfer theories, the model simulates the bidirectional reflectance distribution function based on the canopy architecture at the four scales: (1) tree groups, (2) tree crown geometry, (3) branches, and (4) foliage elements. The model used in this study includes a multiple scattering scheme as described in Chen and Leblanc (2001), which includes all orders of scattering among canopy geometrical structures and is essential for reliable simulations for a wide rage of wavelengths including near infrared. The physical basis of this model provides the generality and accuracy needed for global applications. The major parameters used in the model are crown shape, tree height (stem and canopy), crown diameter, tree density, leaf area index, foliage optical properties, tree group size, branches and shoots, and viewing geometry.

In 4-Scale, the canopy gap fraction distribution with zenith angle is calculated according to the canopy geometry defined by inputs given above. From the input value of LAI and the modeled gap fraction $P(\theta)$ (including gaps within and between tree crowns), the clumping index at various zenith angles (θ) can be calculated as:

$$\Omega = \frac{L_e}{L} \tag{3}$$

where L_e is the effective LAI computed using modified Miller's (1967) theorem (Chen, 1996):

$$L_e = -2\int_0^{\pi/2} \ln[P(\theta)]\cos\theta\sin\theta d\theta \tag{4}$$

In this way, only a single clumping value is produced for a canopy. The clumping index can also be calculated from gap fractions at individual zenith angles, but it generally increases with increasing zenith θ, as found in measurements (Chen, 1996; Leblanc, Chen, Fernandes et al., in press) and modeling (Kucharik et al., 1997). Using Eqs. (3) and (4), the problem of clumping variation with zenith angle is avoided.

The simulations were aimed at covering a wide range of forest characteristics while remaining within reasonable constraints (see Table 1 for input parameters to 4-Scale and their values). Three geometric representations for the envelope of the tree crown are modeled, as this has been found to be an important parameter for BRDF inversion (Rautiainen et al., 2004). Needleleaf species were modeled using a combination of cylinder and cone (Chen & Leblanc, 1997), which is slightly different from other studies using the cone shape (e.g., Li & Strahler, 1992), and broadleaved species are modeled using full ellipsoids (Bartelink, 1998; Nilson & Peterson, 1991; Strahler & Jupp, 1990) as well as half ellipsoids to represent frequently observed reality. While a full ellipsoid has been commonly used in models of deciduous vegetation, a half ellipsoid was also tested as a common crown shape. The optical properties (reflectance and transmittance) of leaves/needles and the background were varied within a reasonable range for the two spectral bands under consideration. While the simulation assumes a homogenous stand of vegetation in terms of the parameters provided, the model contains several parameters that allow for the simulation of clustering at the leaf, shoot, and tree level, which were varied to simulate stands ranging from random to highly clustered distributions. To limit the parameter combinations to reasonable ranges, the tree crown radius has a limit determined by an equation (Table 1) according to stem density and the vertically projected crown coverage. To restrict the foliage distribution, any simulations with a calculated clumping index of greater than one were not included. The 4-Scale model was also used to

Table 1
Input parameters to 4-Scale and their values used in modeling

Parameter	Unit	values
Stand density (χ)	Trees/ha	1000, 2000, 3000, 4000, 6000, 8000, 12,000
Leaf area index	m^2/m^2	0.5, 1, 2, 4, 8
Crown base height	m	1, 5, 10
Crown vertical dimension	m	5, 10, 20
Crown radius (r)	m	Adjusted to achieve vertical crown coverages (C) of 10%, 25%, 50%, 75%, and 100% based on $10^{-4}\pi r^2\chi \le C$
Clumping index (Ω)	dimensionless	0.5, 0.8
Neyamnn clustering	dimensionless	1, 2, 3
Solar zenith angle	degree	10, 15, 20, 25, 30, 35, 40, 45, 50, 55, 60
Leaf reflectance in NIR	dimensionless	0.4, 0.6
Leaf reflectance in red	dimensionless	0.04, 0.06, 0.08
Background reflectance in NIR	dimensionless	0.05, 0.25, 0.5
Background reflectance in Red	dimensionless	0.05, 0.25, 0.5

model the directional reflectance along the principal plane for grassland. Although the model was not specifically designed for this task, the tree parameters were chosen such that they approximate a single grass blade with a density of between 10,000 and 30,000 blades per 10 m^2 area, and a radius for the spheroid shape of between 2 mm and 10 mm to achieve area coverage between 10% and 95%.

The 8 months of global POLDER 1-Level 2 data were obtained from CNES, France, where they were pre-processed with an improved algorithm for atmospheric correction and cloud removal. The POLDER reference grid is based on the sinusoidal equal area projection (Sanson-Flamsted) with a constant resolution along a meridian of 1/18°. All results are presented in this format. The POLDER directional reflectance measurements for land data products include surface reflectance at 443 nm, 565 nm, 670 nm, 765 nm, and 865 nm, as well as polarized reflectance at 865 nm. Only the reflectance at 670 nm and 865 nm in conjunction with the viewing geometry was used here and will be referred to as Red and NIR, respectively. Before extraction of the hotspot and darkspot reflectance, the data were screened to eliminate snow cover and other extreme observations (where NDVI was more than 2 standard deviations from the average).

The interpolation of the hotspot reflectance from available measurements was based on the hotspot model (Chen & Cihlar 1997)

$$F(\xi) = C_1 e^{-C_2 \xi/\pi} \tag{5}$$

where C_1 determines the magnitude of the hotspot, C_2 controls the width of the hotspot, and ξ is the scattering angle, i.e., the angle between illumination and observation. For the calculation of the angular index NDHD, this simple model can be used to estimate the hotspot magnitude, if sufficient observations close to the hotspot exist. The darkspot was chosen as the minimum reflectance observed along the principal plane. The validity of this interpolation was tested using the 4-Scale model, where the method was simulated with data from the forward scattering range along the principal plane between 5° and 30° of the scattering angle and compared to the calculated reflectance at the hotpot. Another method of finding the hotspot used by Leblanc, Chen, White et al. (in press) is the 4-Kernel model based on 4-Scale (White et al., 2001, 2002).

The angular index, NDHD, was consequently calculated on a monthly basis using all observations within 30° of the principal plane in the forward scattering direction for the period from November 1996 to June 1997. The clumping index was calculated according to the regression results from simulations taking into account the solar zenith angle (SZA) and the dominant land cover. The land cover information was obtained from the Global Land Cover map at 1 km resolution (GLC2000 database) aggregated to the POLDER full resolution grid differentiating between needleleaf and broadleaf forests. The regression applicable to the cone/cylinder crown shape was used for those pixels where needleleaf forest dominates; and the regression for ellipsoid shaped trees was applied to all other land cover classes with tree or shrub cover. Areas dominated by non-forest and non-shrub cover types were also included in the resulting clumping index map despite uncertainties in the interpretation of the angular index over these areas. After analyzing monthly clumping index maps for temporal trends, the minimum index value, corresponding to the maximum level of clumping observed in the time period, was represented in the final product.

3. Results and discussion

The importance of several input parameters on the relationship between NDHD and Ω based on 4-Scale simulations is illustrated in Fig. 1. The coverage parameter (A) denotes the vegetation coverage by tree crown envelopes and not by the foliage (there may be small gaps within the tree crowns). With decreasing canopy coverage, the range of clumping index values diminishes. In other words, if there are few structures where the available leaf area can be distributed, then the distribution must necessarily be highly clumped (a low index value).

When canopy coverage is greater than 25% (Fig. 1B–D), the overall correlation is strong (r^2=0.74 and r^2=0.71 for NIR and Red, respectively) with a standard error in clumping index of 0.08. The total number of trees per hectare (Fig. 1B) is of little significance, except that large values of NDHD are less likely for high densities as the crown size diminishes with an increasing number of stems beyond forest closure. Similarly, the range of NDHD values for a small leaf area index (Fig. 1C) is narrow despite a significant range of clumping index (Ω in [0.55,1] for LAI=0.5). As the LAI increases, the range of NDHD increases substantially, although this is difficult to see in Fig. 1C where these points are largely hidden. The minimum NDHD in this plot for a LAI of 8 is 0.43 and 0.53 in NIR and Red, respectively. The canopy height in the range from 5 m to 15 m (Fig. 1D) has virtually no effect on the relationship, although its effect is expected to be significant when the height is lower than 3 m (not shown). The trunk height, which is a separate input parameter, was tested for 1 to 10 m (not shown here) without any bearing on the relationship.

The effect of variations in reflectance of foliage and background on the NDHD is minimized through the nature of the index, but not completely eliminated. A variation in background reflectance in Red from 5% to 50% representing the extreme values for green grass and bright soil, respectively, produces a large difference in the relationship. With increasing background reflectance, the correlation coefficient is reduced considerably with a significant change in the slope of the regression line. The same variation has no discernible effect in NIR where foliage reflectance is much higher than that in Red. Variation of foliage reflectance through possible values for vegetation (NIR: 40–60%; Red: 4–8%), however, results in a decrease of the modeled

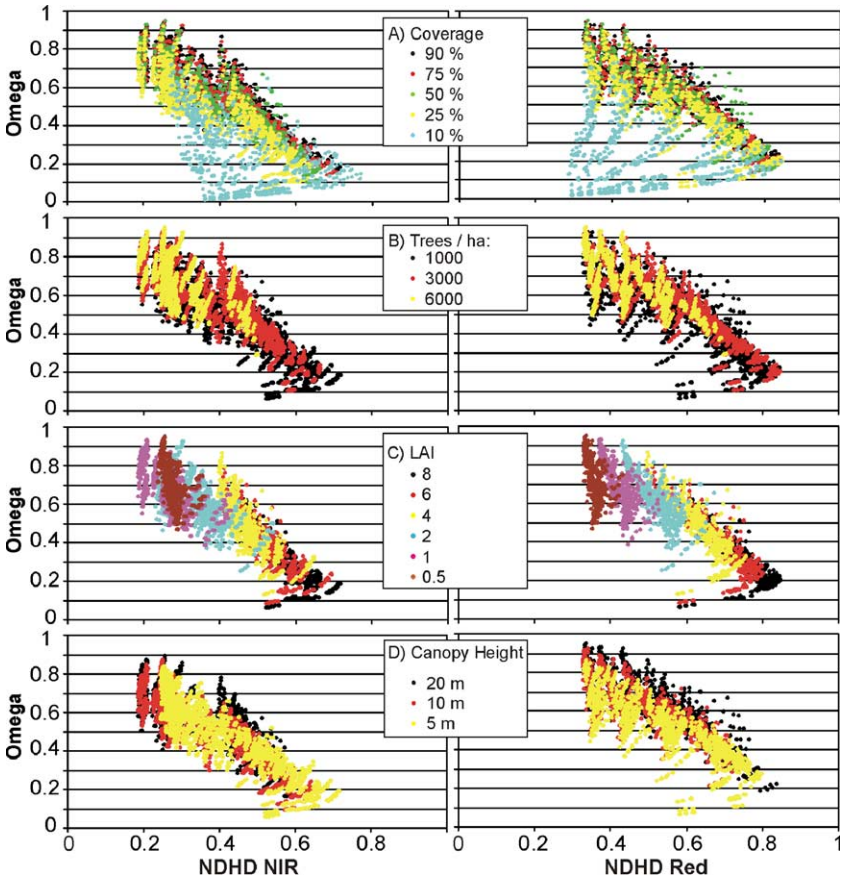

Fig. 1. Modeled NDHD vs. clumping index (Ω) for a wide range of parameters highlighting the distributions of individual parameters within the cluster. The SZA was chosen as 35° for all simulations.

NDHD value of up to 0.1 (with other parameters unaltered) and a negligible effect in the Red band.

The importance of the tree envelope shapes and the solar zenith angle (SZA) was investigated, and the results are shown in Fig. 2 for NIR. While there is little difference between a full and half ellipsoid in modeling broadleaf trees, the cone/cylinder shape assumed for needleleaf trees produces a distinct relationship between the variables for all SZAs. Increasing the SZA has the effect of compressing the range of NDHD values along with a shift towards larger values. The coefficients of the regression lines for the two distinct crown shapes are plotted against the sun angle in Fig. 3. The change of coefficients can be approximated by a quadratic fit. The results for the Red band are analogous to the NIR results and are not shown here. At large SZAs, two distinct clusters emerge for Conifer instead of a single linear relationship. This significantly reduces the correlation as listed in Table 2. The results for relationship between NDHD and clumping index as modeled for Grassland are also shown in Fig. 2. The clumping index does exhibit sensitivities to parameter variations and is in line with the forest results for the spheroid tree model at all solar angles. The high clumping index for grassland conforms to expectations of less clumping for this land cover.

The validity of using the simplified hotspot equation to interpolate was verified by the high correlation between the hotspot reflectance derived from the 4-Scale model and the interpolated hotspot reflectance using the modeled reflectance values with a scattering angle between 5° and 30° (Fig. 4). Fig. 5 depicts examples for selected cover types of the directional reflectance measured by the POLDER instrument during a single month along the principal plane. The reflectance values are graphed against the scattering angle, rather than the viewing angle as the solar angle varies between separate views of the satellite. The magnitude of the hotspot (scattering angle = 0°) in NIR is highest for the dense evergreen broadleaf vegetation and lowest for the coniferous forest with low values in the Red band. A lower NIR reflectance and a higher Red reflectance are observed for the Herbaceous and Shrub cover due to greater background contributions. More importantly, however, the difference between the hotspot and darkspot is larger for the forested samples indicating higher levels of foliage clumping captured in the NDHD index. In the backscattering direction (negative scattering angle) the observations for forested land cover display a pattern that is not explained by model simulations and were consequently excluded from the retrieval of the NDHD index.

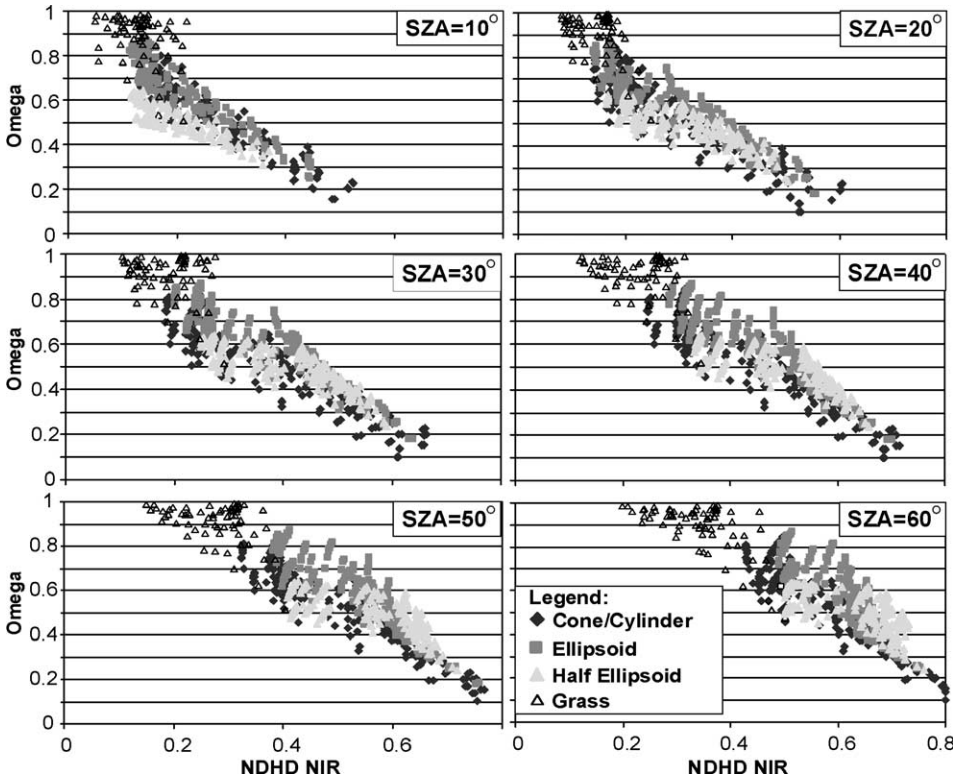

Fig. 2. Modeled NDHD vs. clumping index (Ω) for a range of parameters covering the full range for both variables to highlight the effect of crown shape and solar illumination angle as well as the results for Grassland.

The clumping index calculated on a monthly basis was found to vary through the 8 month period with available data. Table 3 provides a list of global averages of the minimum, maximum, and mean clumping index values derived by land cover (Global Land Cover, 2000 database). These global averages were compared to averages derived from the northern latitudes, equatorial region, and southern latitudes delineated by the tropic of Capricorn and Cancer. The average values for these regions were found to be the same (to 2 decimal places accuracy) as the global averages and only the latter is reported here. A change in the clumping index should have a relationship to actual changes in vegetation. The change in clumping index was therefore calculated to investigate trends. For each land cover class, all pixels that had at least one valid clumping index retrieval in the November–January and April–June period were used

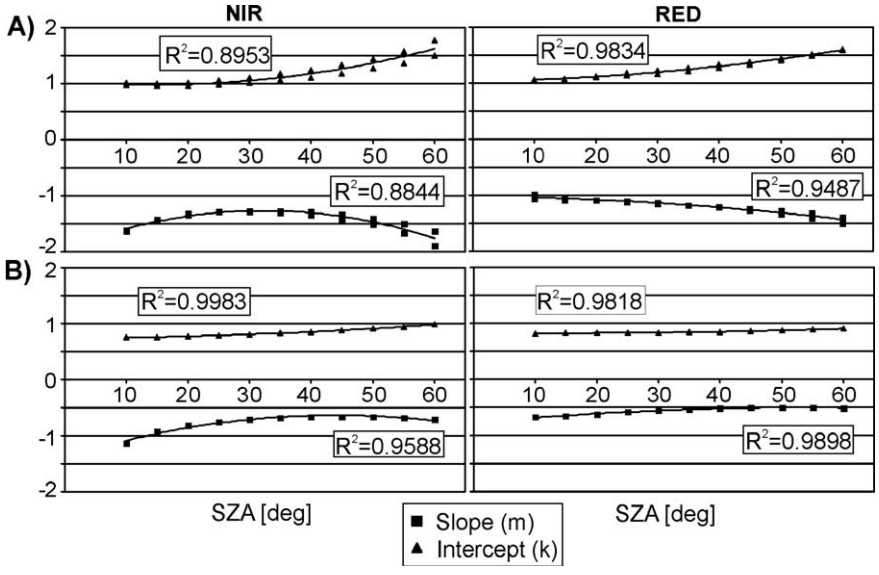

Fig. 3. Coefficients of the regression $\Omega = m'\,\mathrm{NDHD} + k$ vs. solar zenith angle (SZA) for (A) half and full ellipsoid and (B) cone/cylinder, where m is negative and k positive. The correlation coefficients (RZ) for a second-order polynomial fit are shown.

Table 2
The linear coefficients of the line of best fit for NDHD vs. Ω (Ω = A * NDHD + B) at a range of sun angles and two wavelengths (Red = 670 nm, NIR = 865 nm)

SZA (deg)	Cone/cylinder			Ellipsoid			Half ellipsoid		
	A	B	R^2	A	B	R^2	A	B	R^2
Red									
10	−0.61	0.76	0.63	−1.02	1.02	0.89	−1.08	1.06	0.89
15	−0.62	0.77	0.65	−1.04	1.03	0.91	−1.08	1.05	0.87
20	−0.58	0.78	0.62	−1.08	1.08	0.91	−1.08	1.06	0.88
25	−0.54	0.78	0.58	−1.12	1.13	0.89	−1.10	1.09	0.88
30	−0.51	0.78	0.54	−1.15	1.18	0.87	−1.13	1.13	0.88
35	−0.49	0.78	0.51	−1.18	1.23	0.83	−1.17	1.18	0.87
40	−0.48	0.79	0.48	−1.20	1.28	0.80	−1.22	1.23	0.87
45	−0.47	0.80	0.45	−1.23	1.34	0.77	−1.27	1.29	0.86
50	−0.46	0.81	0.42	−1.27	1.40	0.73	−1.33	1.36	0.84
55	−0.47	0.83	0.40	−1.32	1.47	0.70	−1.40	1.45	0.83
60	−0.48	0.85	0.37	−1.40	1.57	0.66	−1.51	1.56	0.82
NIR									
10	−0.98	0.70	0.73	−1.50	0.96	0.86	−1.50	0.94	0.88
15	−0.87	0.71	0.71	−1.38	0.94	0.86	−1.40	0.91	0.83
20	−0.77	0.72	0.69	−1.29	0.97	0.86	−1.30	0.91	0.84
25	−0.70	0.74	0.65	−1.26	1.01	0.85	−1.25	0.94	0.85
30	−0.66	0.76	0.62	−1.27	1.06	0.84	−1.24	0.97	0.85
35	−0.63	0.77	0.58	−1.29	1.13	0.83	−1.24	1.01	0.86
40	−0.61	0.79	0.55	−1.34	1.20	0.81	−1.27	1.07	0.87
45	−0.61	0.82	0.52	−1.40	1.28	0.80	−1.31	1.13	0.87
50	−0.61	0.84	0.48	−1.50	1.39	0.78	−1.38	1.22	0.88
55	−0.63	0.87	0.44	−1.67	1.54	0.76	−1.49	1.33	0.86
60	−0.66	0.92	0.39	−1.90	1.74	0.74	−1.62	1.46	0.87

to determine an average monthly trend for northern latitudes, equatorial region, and southern latitudes, with the results being presented in Table 3. No result is reported for land cover types where less than 100 valid samples could be retrieved in a region. The lowest monthly changes occurred in the equatorial region, and the magnitude of change was approximately equal to the northern and southern latitudes but opposite in sign. All trends in the northern latitudes were negative, which indicates a decrease in clumping index from December to June suggesting an increased level of clumping in accordance with plant growth patterns. For the southern latitudes the positive trends indicate a greater level of clumping during the November–January period. The 'deciduous, needleleaf' class showed nearly 3 times the magnitude of change as the 'evergreen, needleleaf' class in the northern region as did the 'broadleaf, deciduous, closed' class in comparison to the 'broadleaf, evergreen' class. This was not true for the southern region, however, where the values were nearly the same. The 'broadleaf, deciduous, open' class exhibited little change in all regions, possibly because the increase in leaf area was more localized and had less importance in determining the hotspot and darkspot reflectance. Significant trends were also present in the Shrub and Herbaceous classes, which may be interpreted as the clumping index responding to phenological changes in these environments. However, the magnitudes of change indicated for the classes 'Tree Cover, burnt' and 'Bare Area' were also significant, suggesting that either vegetation growth or changes in topographic shadows with sun angle may be responsible. The effect of solar zenith angle on vegetation clumping retrieval is considered in our algorithm, but this effect on bare surface with topography may not be entirely removed.

A global map of the vegetation clumping index is shown in Fig. 6 and represents the minimum index value (maximum clumping) from the 8 months of data for vegetated cover types as highlighted by the shaded classes in Table 3. The 'Shrub' and 'Grassland' classes were retained, as the modeling results for broadleaf trees can be extended to these classes (Fig. 2), albeit some inconsistency between these classes at small SZAs. The model suggests, however, that in sparse vegetation the clumping effect may be exaggerated. Areas with less than 25% vegetation coverage should, therefore, be treated with some caution. Only NIR data are used in deriving this map. While the angular index NDHD minimizes the effect of foliage and background reflectance, the latter was found to influence the relationship in the Red band more than in the NIR band. This, coupled with the greater uncertainty in the atmospheric correction in the Red band, led to the choice of the NIR band for global clumping index retrieval. However, strong multiple scattering in NIR within vegetation decrease the shadow darkness, making NIR less sensitive to vegetation structure. In airborne applications, where the atmospheric effect is small, Red wavelengths may have advantages over NIR wavelengths for vegetation structure mapping.

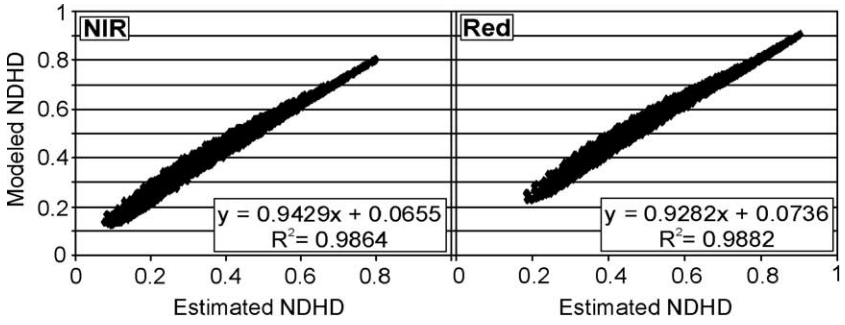

Fig. 4. Estimated NDHD using the simplified hotspot model compared with 4-Scale modeled data between 5° and 30° scattering angle.

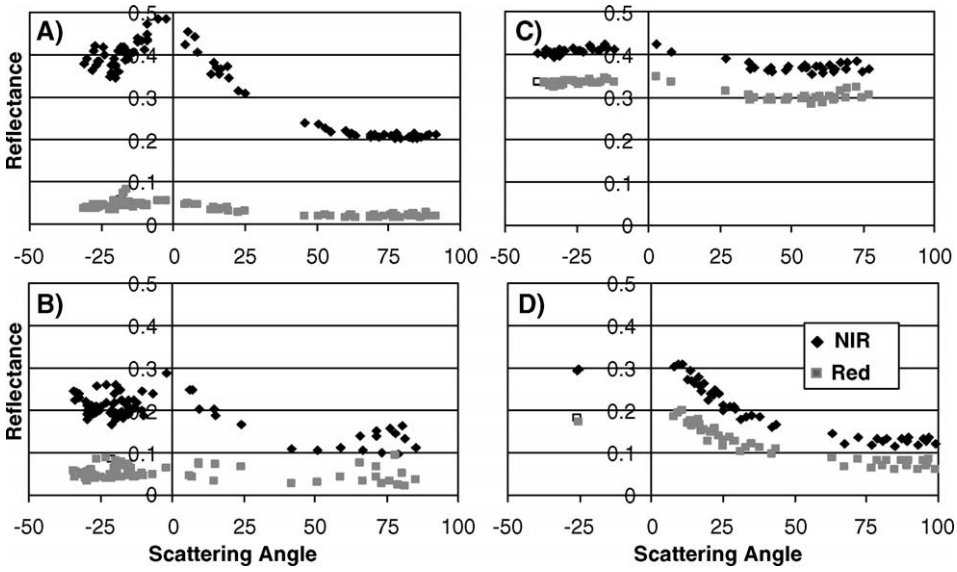

Fig. 5. POLDER (NIR and Red) directional reflectance from June 1997 along the principal plane for a single resolution element in (A) broadleaved, evergreen; (B) needle-leaved, evergreen; (C) herbaceous cover, open; and (D) shrub cover, deciduous; land cover types (GLC, 2000). A negative scattering angle was assigned to indicate the backscattering direction.

This global clumping index map is, for the first time, derived using multi-angular POLDER data assisted by a geometrical optical model. It can be an equally important input to global carbon and water cycle models compared with other structural parameters such as the leaf area index. The use of this parameter allows for improved estimation of radiation interception and distribution within plant canopies, particularly important for models with sunlit and shaded leaf stratification (Chen et al., 2003). However, the clumping index map presented here has several limitations. First, the spatial resolution is low. At the 7 km resolution, most pixels have mixed land covers. Although the algorithm for retrieving the clumping index does not differ largely among cover types, the variation in cover types, especially height of vegetation, can cause additional shadows that are not modeled since the model assumes homogeneous vegetation cover without uncharacteristic height variations. Shadows at the edge of newly disturbed areas in some cases are

Table 3
Average statistics for the clumping index values calculated by for the period November 1996 to June 1997

Class	Class names	Min	Max	Mean	d - NL	d - EQ	d - SL
1	Tree Cover, broadleaf, evergreen	0.59	0.68	0.63	-0.006	-0.004	0.024
2	Tree Cover, broadleaf, deciduous, closed	0.59	0.79	0.69	-0.019	-0.001	0.021
3	Tree Cover, broadleaf, deciduous, open	0.62	0.78	0.70	-0.005	0.007	0.025
4	Tree Cover, needleleaf, evergreen	0.55	0.68	0.62	-0.012	-0.017	0.009
5	Tree Cover, needleleaf, deciduous	0.60	0.77	0.68	-0.033	N/A	N/A
6	Tree Cover, mixed leaf type	0.58	0.79	0.69	-0.024	-0.018	0.011
7	Tree Cover, regularly flooded, fresh water	0.61	0.69	0.65	N/A	-0.002	N/A
8	Tree Cover, regularly flooded, saline water	0.65	0.79	0.72	N/A	-0.006	N/A
9	Mosaic: Tree Cover / Other natural vegetation	0.64	0.82	0.72	-0.013	0.008	N/A
10	Tree Cover, burnt	0.65	0.86	0.75	-0.036	N/A	N/A
11	Shrub Cover, closed-open, evergreen	0.62	0.80	0.71	-0.020	-0.010	0.024
12	Shrub Cover, closed-open, deciduous	0.62	0.80	0.71	-0.016	0.009	0.022
13	Herbaceous Cover, closed-open	0.64	0.83	0.74	-0.016	0.003	0.026
14	Sparse herbaceous or sparse shrub cover	0.67	0.84	0.75	-0.019	0.008	0.024
15	Reg. flooded shrub and/or herbaceous cover	0.68	0.85	0.77	-0.026	0.004	0.024
16	Cultivated and managed areas	0.63	0.83	0.73	-0.018	-0.006	0.026
17	Mosaic: Cropland / Tree Cover / Natural veg	0.64	0.76	0.70	-0.011	-0.004	0.024
18	Mosaic: Cropland / Shrub and/or grass cover	0.65	0.81	0.73	-0.018	0.001	0.026
19	Bare Areas	0.75	0.99	0.87	-0.032	-0.03	0.027

The minimum, maximum and mean values are global averages from all valid retrievals and the change per month (d) derived from a regression of the index values for all pixels where at least one value per season was retrieved is given for the northern latitudes (NL), the equatorial region (EQ), and the southern latitudes (SL). Shading indicates that the class is included in the final product and 'N/A' indicates lack of samples.

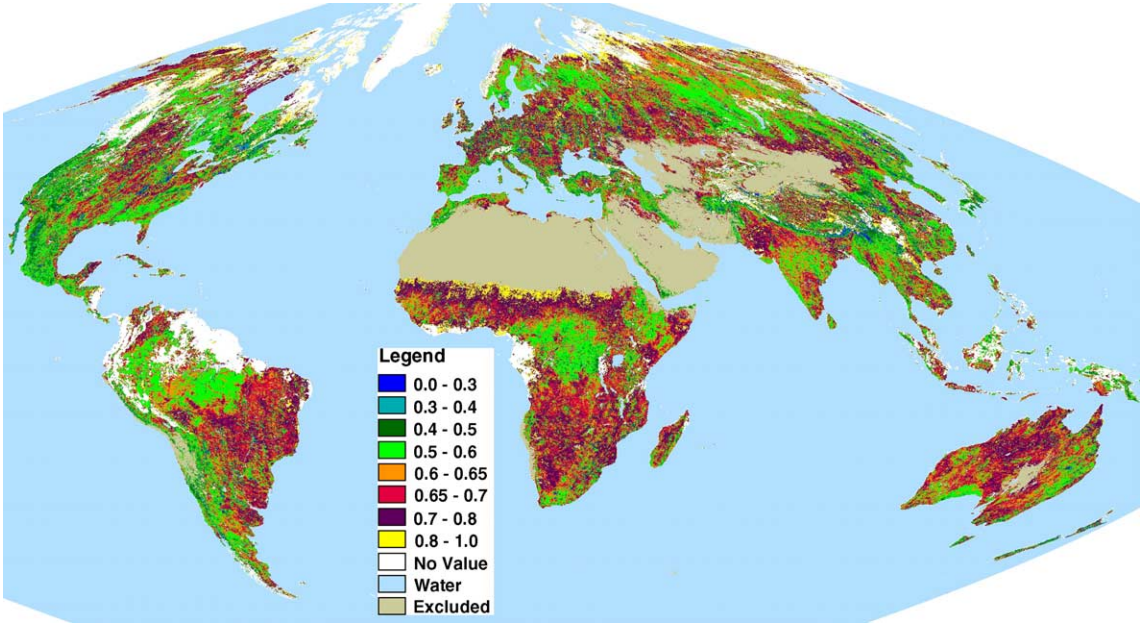

Fig. 6. Global vegetation clumping index map derived from POLDER 1 data using the normalized difference between interpolated hotspot and darkspot NIR reflectance and applied to vegetated land cover. Vegetation clumping increases with decreasing values of the index.

particularly important relative to the overall scene reflectance (Asner et al., 2003). Second, in mountainous and hilly regions, terrain-induced shadows can also enhance the BRDF variation (Sandmeier & Itten, 1997; Schaaf et al., 1994; Richter, 1998), and this effect is not yet removed from the current map. As many forests are located in hilly regions, the retrieved clumping index may be negatively biased (i.e., more clumped than reality). To address the first limitation, POLDER data can be used in conjunction with high-resolution imagery to characterize the sub-pixel land cover variation, or to conduct spectral unmixing to estimate cover fractions within POLDER pixels using existing methodologies such as that applied to MODIS (Hansen et al., 2003). However, the ultimate way to improve clumping mapping is to acquire multiple angle imagery at high spatial resolution, a direction to pursue in earth observation if we are fully convinced for the importance of vegetation structure in ecological functioning and modeling. To reduce the second limitation, further modeling can be readily made using high resolution DEM data.

4. Conclusion

In this study, the BRDF of vegetated land surfaces was used to extract vegetation structural information globally using multi-angular data from the POLDER instrument. The relationship between the angular index NDHD, which is the normalized difference between the reflectance at the hotspot in the backward scattering direction and at the darkspot in the forward direction along the principal plane, and the clumping index of vegetation was examined using the 4-Scale model. The relationship was found to be significant for the Red and NIR wavelengths when the crown envelope coverage of the ground in a forest stand exceeds 25%, even though other forest structural parameters are allowed to vary in large ranges. The relationship between the two indices was also found to be dependent on the solar angle and the modeled crown shape. The slope and intercept of the regression line were determined as a function of solar angle, and the two cone/cylinder shapes assumed for coniferous vegetation were treated distinctly from the full/half spheroid shape assumed for all trees according to the global land cover map (GLC, 2000).

The absence of direct satellite measurements at the hotspot requires modeling of the hotspot signature, which was achieved by fitting an exponential function, a simplified hotspot model, (Chen & Cihlar, 1997) to observations within 30° of the hotspot. A highly significant correlation was found when this approach was tested against model simulations. The POLDER data were screened to remove snow covered and spurious observations and divided into monthly aggregates. For each month of the satellite observations (November 1996–June 1997) the clumping index was calculated and the temporal changes were extracted for the distinct land cover types. Temporal changes in the clumping index were evident with the average changes corresponding to the maximum clumping during the peak growing season (Chen, 1996). The clumping map was found to exhibit evidence of dependence on topography in mountainous regions as well as very sparsely vegetated regions, which must be excluded. The final clumping index map reflects the greatest level of clumping observed over the time period. Further ground validation, relating field measurements of clumping index to high or intermediate resolution multi-angular data, such as

airborne campaigns, would be desirable for a variety of ecosystems and in particular for a variety of topographic conditions. Our research may provide impetus to such projects as well as improvement of space missions acquiring directional reflectance in close vicinity of the hotspot and at a higher spatial resolution than POLDER.

Acknowledgements

We are grateful to CNES for the provision of re-processed POLDER 1 data. The research was funded through a research grant from the Natural Science and Engineering Research Council of Canada. The clumping index map shown here can be provided on request.

References

Asner, G. P., Bustamate, M. M. C., & Townsend, A. R. (1996). Scale dependence of biophysical structure in deforested areas bordering the Tapajos National Forest, Central Amazon. *Remote Sensing of Environment*, *87*, 507–520.

Asner, G. P., Wessman, C. A., Schimel, D. S., & Archer, S. (1998). Variability in leaf and litter optical properties: Implications for BRDF model inversions using AVHRR, MODIS, and MISR. *Remote Sensing of Environment*, *63*, 243–257.

Bacour, C., Jacquemoud, S., Tourbier, Y., Dechambre, M., & Frangi, J.-P. (2001). Design and analysis of numerical experiments to compare four canopy reflectance models. *Remote Sensing of Environment*, *79*, 72–83.

Baldocchi, D. D., Wilson, K. B., & Gu, L. (2002). How the environment, canopy structure and canopy physicalogical functioning influence carbon, water and energy fluxes of a temperate broad-leaved deciduous forest—an assessment with the biophysical model CANOAK. *Tree Physiology*, *22*, 1065–1077.

Bartelink, H. H. (1998). Radiation interception by forest trees: A simulation study on effects of stand density and foliage clustering on absorption and transmission. *Ecological Modeling*, *10*, 213–225.

Bernier, P. Y., Raulier, F., Stenberg, P., & Ung, C. H. (2001). Importance of needle age and shoot structure on canopy net photosynthesis of balsam fir (*Abies balsamea*): A spatially inexplicit modeling analysis. *Tree Physiology*, *21*, 815–830.

Cescatti, A. (1998). Effects of needle clumping in shoots and crowns on the Radiative Regime of a Norway Spruce Canopy. *Annales des Sciences Forestières*, *55*, 89–102.

Chen, J. M. (1996). Optically-based methods for measuring seasonal variation in leaf area index of boreal conifer forests. *Agricultural and Forest Meteorology*, *80*, 135–163.

Chen, J. M., & Black, T. A. (1992). Defining leaf area index for non-flat leaves. *Plant Cell & Environment*, *15*, 421–429.

Chen, J. M., & Cihlar, J. (1997). A hotspot function in a simple bi-directional reflectance model for satellite applications. *Journal of Geophysical Research*, *102*, 25907–25913.

Chen, J. M., & Leblanc, S. G. (1997). A four-scale bidirectional reflectance model based on canopy architecture. *IEEE Transactions on Geoscience and Remote Sensing*, *35*, 1316–1337.

Chen, J. M., & Leblanc, S. G. (2001). Multiple-scattering scheme useful for geometric optical modeling. *IEEE Transactions on Geoscience and Remote Sensing*, *39*, 1061–1071.

Chen, J. M., Liu, J., Chilar, J., & Goulden, M. L. (1999). Daily canopy photosynthesis model through temporal and spatial scaling for remote sensing applications. *Ecological Modeling*, *124*, 99–119.

Chen, J. M., Pavlic, G., Brown, L., Cihlar, J., Leblanc, S. G., White, H. P., et al. (2002). Validation of Canada-wide leaf area index maps using ground measurements and high and moderate resolution satellite imagery. *Remote Sensing of Environment*, *80*, 165–184.

Chen, J. M., Liu, J., Leblanc, S. G., Lacaze, R., & Roujean, J.-L. (2003). Multi-angular optical remote sensing for assessing vegetation structure and carbon absorption. *Remote Sensing of Environment*, *84*, 516–525.

Chen, J. M., Liu, J., Leblanc, S. G., Roujean, J.-L., & Lacaze, R. (2001). *Utility of multi-angle remote sensing for terrestrial carbon cycle modeling*. Proceedings of the 8th International Symposium on Physical Signatures and Measurements in Remote Sensing, Aussois, France, 8–13 January.

Cierniewski, J., Gdala, T., & Karnieli, A. (2004). A hemispherical-directional reflectance model as a tool for understanding image distinctions between cultivated and uncultivated bare surfaces. *Remote Sensing of Environment*, *90*, 505–523.

Deering, D. W., Eck, T. F., & Banerjee, B. (1999). Characterization of the reflectance anisotropy of three boreal forest canopies in spring–summer. *Remote Sensing of Environment*, *67*, 205–229.

Diner, D., Beckert, J. C., Bothwell, G. W., & Rodriguez, J. I. (2002). Performance of the MISR instrument during its first 20 months in earth orbit. *IEEE Transactions on Geoscience and Remote Sensing*, *40*, 1449–1466.

Gao, F., Schaaf, C. B., Strahler, A. H., Jin, Y., & Li, X. (2003). Detecting vegetation structure using a kernel-based BRDF model. *Remote Sensing of Environment*, *86*, 198–205.

Gerard, F. F., & North, P. R. J. (1997). Analyzing the effect of structural variability and canopy gaps on forest BRDF using a geometric-optical model. *Remote Sensing of Environment*, *62*, 46–62.

Gobron, N., Pinty, B., Verstraete, M. M., & Govaerts, Y. (1997). Theoretical limits to the estimation of the leaf area index on the basis of visible and near-infrared remote sensing data. *IEEE Transactions on Geoscience and Remote Sensing*, *35*, 1438–1445.

Gobron, N., Pinty, B., Verstraete, M. M., Widlowski, J.-L., & Diner, D. (2002). Uniqueness of multiangular measurements—Part II: Joint retrieval of vegetation structure and photosynthetic activity from MISR. *IEEE Transactions on Geoscience and Remote Sensing*, *40*, 1574–1592.

Global Land Cover 2000 database. European Commission, Joint Research Centre, 2003. http://www.gvm.jrc.it/glc2000.; Jupp, D. L. B., & Strahler, A. H. (1991). A hotspot model for leaf canopies. *Remote Sensing of Environment*, *38*, 193–210.

Hansen, S. C., DeFries, R. S., Townshend, J. R. G., Carroll, M., Dimiceli, C., & Sohlberg, R. A. (2003). Global percent tree cover at a spatial resolution of 500 meters: First results of the MODIS vegetation continuous fields algorithm. *Earth Interactions*. September 9, 2003.

Hapke, B., DiMucci, D., Nelson, R., & SMythe, W. (1996). The cause of the hot spot in vegetation canopies and soil: Shadow-hiding versus coherent backscatter. *Remote Sensing of Environment*, *58*, 63–68.

Kucharik, C. J., Norman, J. M., Murdock, L. M., & Gower, S. T. (1997). Characterizing canopy nonrandomness with a Multiband Vegetation Imager (MVI). *Journal of Geophysical Research*, *102*, 29455–29473.

Lacaze, R., Chen, J. M., Roujean, J. L., & Leblanc, S. G. (2002). Retrieval of vegetation clumping index using hotspot signatures measured by the POLDER instrument. *Remote Sensing of Environment*, *79*, 84–95.

Leblanc, S. G., Bicheron, P., Chen, J. M., Leroy, M., & Cihlar, J. (1999). Investigation of directional reflectance in boreal forests with an improved 4-scale model and airborne POLDER data. *IEEE Transactions on Geoscience and Remote Sensing*, *37*, 1396–1414.

Leblanc, S. G., Chen, J. M., Fernandes, R., Deering, D. W. & Conley, A. (in press). Methodology comparison for canopy structure parameters extraction from digital hemispherical photography in boreal forests. *Agricultural and Forest Meteorology*.

Leblanc, S. G., Chen, J. M., White, H. P. & Latifvic, R. (in press). Canada-wide foliage clumping index mapping from multi-angular POLDER measurements. *Canadian Journal of Remote Sensing*.

Li, X., & Strahler, A. H. (1992). Geometric-optical bidirectional reflectance modeling of the discrete crown vegetation canopy: Effect of crown shape and mutual shadowing. *IEEE Transactions on Geoscience and Remote Sensing*, *30*, 276–291.

Liu, J., Chen, J. M., Chilar, J., & Chen, W. (2002). Remote sensing-based estimation of net primary productivity over Canadian landmass. *Global Ecology and Biogeography*, *11*, 115–129.

Liu, J., Chen, J. M., & Chilar, J. (2003). Mapping evapotranspiration based on remote sensing: An application to Canada's landmass. *Water Resources Research*, *39*, 1189–1200.

Miller, J. B. (1967). A formula for average foliage density. *Australian Journal of Botany*, *15*, 141–144.

Nilson, T. (1971). A theoretical analysis of the frequency of gaps in plant stands. *Agricultural Meteorology*, *8*, 25–38.

Nilson, T., & Peterson, U. (1991). A forest canopy reflectance model and a test case. *Remote Sensing of Environment*, *37*, 131–142.

Palmroth, S., & Hari, P. (2001). Evaluation of the importance of acclimation of needle structure, photosynthesis, and respiration to available photosynthetically active radiation in a Scots pine canopy. *Canadian Journal of Forest Research*, *31*, 1235–1243.

Panferov, O., Knyazikhin, Y., Myneni, R. B., Szarzynski, J., Engwald, S., Schnitzler, K. G., et al. (2001). The role of canopy structure in the spectral variation of transmission and absorption of solar radiation in vegetation canopies. *IEEE Transactions on Geoscience and Remote Sensing*, *39*, 241–253.

Pinty, B., Widlowski, J.-L., Gobron, N., Verstraete, M. M., & Diner, D. (2002). Uniqueness of multiangular measurements—Part I: An indicator of subpixel surface heterogeneity from MISR. *IEEE Transactions on Geoscience and Remote Sensing*, *40*, 1560–1573.

Rautiainen, M., Stenberg, P., Nilson, T., & Kuusk, A. (2004). The effect of crown shape on the reflectance of coniferous stands. *Remote Sensing of Environment*, *89*, 41–52.

Richter, R. (1998). Correction of satellite imagery over mountainous terrain. *Applied Optics*, *37*, 4004–4015.

Running, S. W., Hunt, E. R., Nemani, R., & Glassy, J. (1994). *MODIS LAI (leaf area index) and FPAR (fraction photosynthetically active radiation), MODIS algorithm document*. NASA, 19 pp.

Sandmeier, S., & Deering, D. W. (1999). Structure analysis and classification of boreal forests using airborne hyperspectral BRDF data from ASAS. *Remote Sensing of Environment*, *69*, 281–295.

Sandmeier, S., & Itten, K. I. (1997). A physically-based model to correct atmospheric and illumination effects in optical satellite data of rugged terrain. *IEEE Transactions on Geoscience and Remote Sensing*, *35*, 708–717.

Schaaf, C. B., Li, X., & Strahler, A. H. (1994). Topographic effects on bidirectional and hemispherical reflectances calculated with a geometric-optical canopy model. *IEEE Transactions on Geoscience and Remote Sensing*, *32*, 1186–1193.

Sellers, P. J., Los, S. O., & Tucker, C. J. (1994). A global $1° \times 1°$ NDVI data set for climate studies. Part 2: The generation of global fields of terrestrial biophysical parameters from the NDVI. *International Journal of Remote Sensing*, *11*, 95–111.

Stenberg, P. (1998). Implications of shoot structure on the rate of photosynthesis at different levels in a coniferous canopy using a model incorporating grouping and penumbra. *Functional Ecology*, *12*, 82–91.

Strahler, A. H., & Jupp, D. L. B. (1990). Modeling bi-directional reflectance of forests and woodlands using Boolean models and geometric optics. *Remote Sensing of Environment*, *34*, 153–166.

Walcroft, A. S., Brown, K. J., Schuster, W. S. T., Tissue, D. T., Turnbull, M. H., Griffin, K. L. & Whitehead, D. (in press). Radiative transfer and carbon assimilation in relation to architecture, foliage area distribution and clumping in a mature temperature rainforest canopy in New Zealand. *Agricultural and Forest Meteorology*.

Wang, Y., Woodcock, C. E., Buermann, W., Stenberg, P., Voipio, P., Smolander, H., et al. (2004). Evaluation of the MODIS LAI algorithm at a coniferous forest site in Finland. *Remote Sensing of Environment*, *91*, 114–127.

White, H. P., Miller, J. R., & Chen, J. M. (2001). Four-scale linear model for anisotropic reflectance (FLAIR) for plant canopies—Part I: Model description and partial validation. *IEEE Transactions on Geoscience and Remote Sensing*, *39*, 1072–1083.

White, H. P., Miller, J. R., & Chen, J. M. (2002). Four-scale linear model for anisotropic reflectance (FLAIR) for plant canopies—Part II: Validation and inversion with CASI, POLDER, and PARABOLA data at BOREAS. *IEEE Transactions on Geoscience and Remote Sensing*, *40*, 1038–1046.

Zhang, Y., Shabanov, N., Knyazikhin, Y., & Myneni, R. B. (2002). Assessing the information content of multiangle satellite data for mapping biomes: II. Theory. *Remote Sensing of Environment*, *80*, 435–446.

Zhang, Y., Tian, Y., Myneni, R. B., Knyazikhin, Y., & Woodcock, C. E. (2002). Assessing the information content of multiangle satellite data for mapping biomes: I. Statistical analysis. *Remote Sensing of Environment*, *80*, 418–434.